

# ADVANCED MATERIALS

## Supporting Information

for *Adv. Mater.*, DOI: 10.1002/adma.202101358

Crystallization by Amorphous Particle Attachment: On  
the Evolution of Texture

*Vanessa Schoeppler, Deborah Stier, Richard J. Best,  
Chengyu Song, John Turner, Benjamin H. Savitzky,  
Colin Ophus, Matthew A. Marcus, Shiteng Zhao, Karen  
Bustillo, and Igor Zlotnikov\**

## Supporting Information

**Crystallization by amorphous particle attachment: On the evolution of texture**

Vanessa Schoeppler, Deborah Stier, Richard J. Best, Chengyu Song, John Turner, Benjamin H. Savitzky, Colin Ophus, Matthew A. Marcus, Shiteng Zhao, Karen Bustillo, Igor Zlotnikov\*

Lattice Rotation Analysis. To further characterize the crystal rotation, a misorientation map was calculated by comparing the lattice orientation of neighboring pixels. According to the color key shown in Figure S1A, orientation changes that result from a rotation around the calcite  $c$ -axis appear as red, rotations around the  $\langle 10\bar{1}0 \rangle$  and  $\langle 1\bar{2}10 \rangle$  axes are displayed as cyan, blue or green. Saturation is correlated to the magnitude of the misorientation angle where no misorientation is displayed as gray. As indicated before, the gradual rotation is clearly distinguishable within the first 50  $\mu\text{m}$  of the prisms due to the homogenous colors, mostly green, blue, and cyan tones, which can be slightly mixed resulting in brighter blue or green tones (Figure S1B-FigureS1E). Considering the symmetry of calcite, this indicates rotations either around one of the  $\langle 1\bar{2}10 \rangle$  axes, or one of the  $\langle 10\bar{1}0 \rangle$  axes, or a combination of both (Figure S1A). No rotations around the  $c$ -axis are visible in the area of gradual rotations. In the area of the sub-domain formation a mixture of rotation axes is present. Areas of both, warmer purple tones and colder blue, green, cyan tones are visible, often following the sub-grain boundaries. The misorientation map further demonstrates that in some prisms the lattice does not rotate (arrows in Figure S1B). Interestingly, the  $c$ -axis of these prisms is close to parallel to the growth axis.

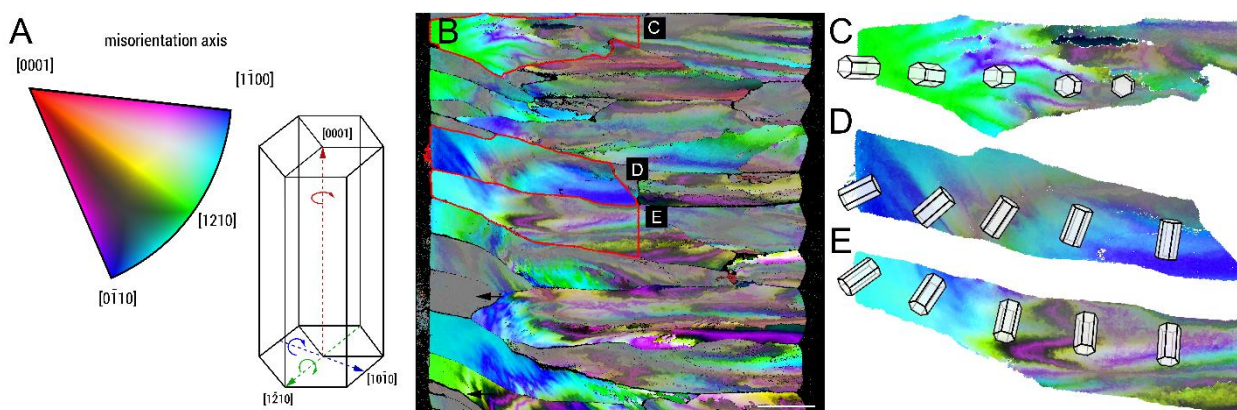


**Figure S1.** Lattice rotation axis analysis in *P. nigra*. (A) Color key for the misorientation axis mapped in B-E and a schematic representation of rotation axes described in the supplementary text. (B) Lattice rotation axes of a section of the shell from *P. nobilis*. Direction of growth is from left to right. Scale bar is 20  $\mu\text{m}$ . (C)-(E) A closer look at lattice rotation axes of three prisms taken from (B).

Organic content analysis. The energy filtered TEM image (EFTEM) in Figure S2A shows 10 to 50 nm sized bright spots that appear within the domains (gray arrows) and at the interfaces (red arrows), indicating areas of decreased density, which could be caused by porosity or the presence of less dense materials, such as organic material. To examine the organic distribution within the domains and the interfaces, scanning transmission X-ray microscopy (STXM) has been performed at the carbon K-edge on a FIB lift-out specimen whose plane is parallel to the prism's growth direction (Figure S2B-S2D). A stack of STXM images was acquired covering a photon energy range from 278 eV to 330 eV. By analyzing this stack, the carbon K-edge spectrum shown in Figure S2B was obtained, which exhibits peaks that can be associated with calcium carbonates and organics.

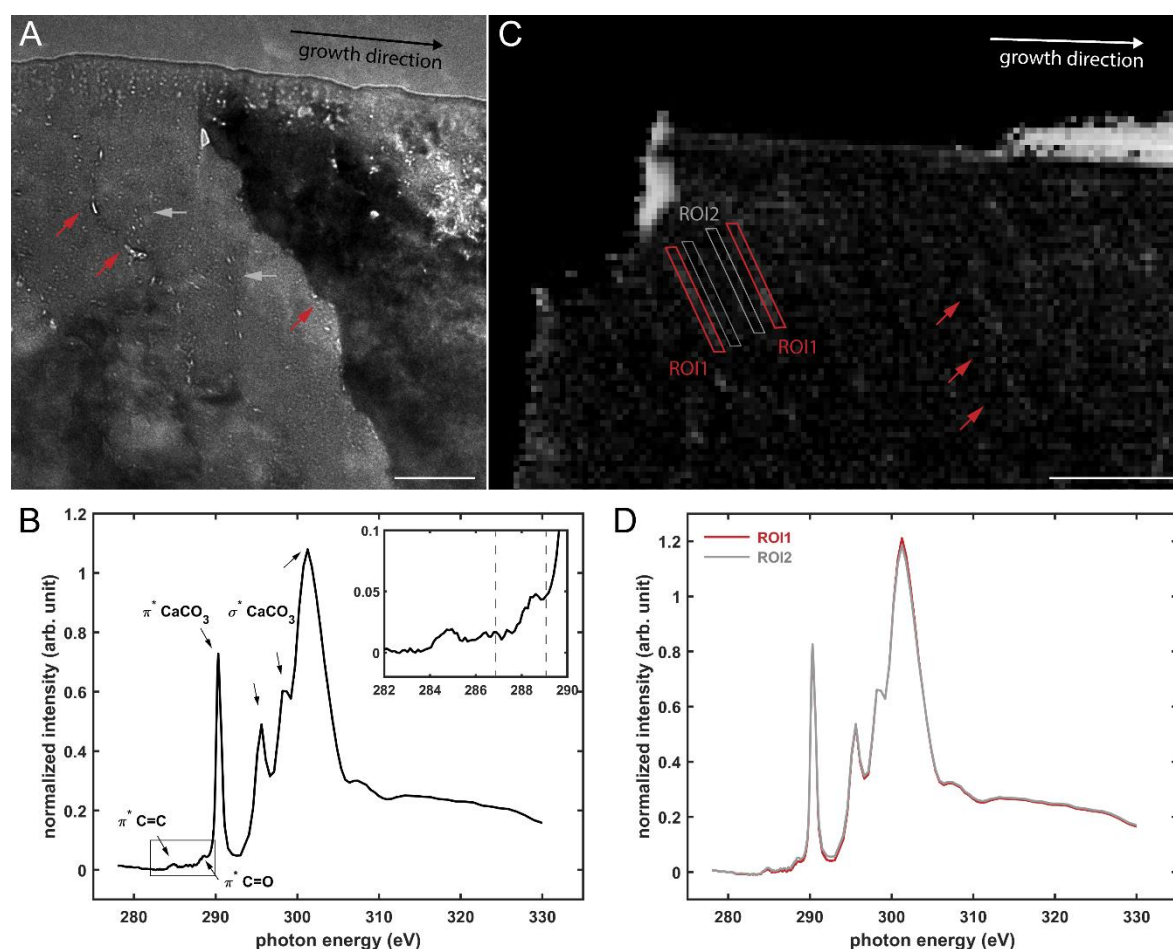


**Figure S2.** Distribution of the organic matter. (A) EFTEM image of a TEM lamella showing several domains. Areas of lower density within the domains and at the interface are marked with gray and red arrows, respectively. Scale bar is 200 nm. (B) K-edge carbon spectrum of the entire STXM stack consisting of images corresponding to the area imaged in C. (C) Average optical-density image of a different lamella covering photon energies from 287 eV to 289 eV, as indicated in the inset in B. The area that corresponds to the interfaces is marked in red (ROI1) and the regions next to the interfaces are marked in gray (ROI2). Scale bar is 1  $\mu$ m. (D) K-edge carbon spectra of the regions of interest marked in C.

While the strong  $\pi^*$  peak at 290.3 eV and the three following  $\sigma^*$  post-edge peaks at 295.6 eV, 298.2 eV and 301.3 eV are associated to the CO<sub>3</sub> carbonate bond, the small  $\pi^*$  peak at 288.4 eV can be linked to the C=O amide and carboxylate bonds in organic molecules.<sup>[61]</sup> Figure S2C is an average intensity projection of the STXM images from 287 eV to 289 eV, representing the organic peak (inset in Figure S2B) and showing the upper edge of the lift-out specimen. Here, brighter areas signify higher organic content, except for the white layer in the upper right corner, which is the highly absorbing platinum layer—a remnant of the FIB-procedure. The sample exhibits thin elongated regions with slightly increased intensity, oriented at a similar angle as the interfaces (red arrows). In Figure S2D two spectra are depicted that correspond to the regions marked in Figure S2C, showing that the organic peak can be detected in both regions—the area that is assumed to correspond to the interfaces (red ROI1) and the regions next to the interfaces (gray ROI2).

- [61] G. D. Cody, H. Ade, C. M. O. D. Alexander, T. Araki, A. Butterworth, H. Fleckenstein, G. Flynn, M. K. Gilles, C. Jacobsen, A. L. D. Kilcoyne, K. Messenger, S. A. Sandford, T. Tyliczszak, A. J. Westphal, S. Wirick, H. Yabuta, *Meteorit. Planet. Sci.* **2008**, *43*, 353.